The Amino-Terminal PrP Domain Is Crucial to Modulate Prion Misfolding and Aggregation

Yraima Cordeiro,* Julia Kraineva,† Mariana P. B. Gomes,* Marilene H. Lopes,‡ Vilma R. Martins,‡ Luís M. T. R. Lima,§ Débora Foguel,* Roland Winter,† and Jerson L. Silva*

*Instituto de Bioquímica Médica, Centro Nacional de Ressonância Magnética Nuclear de Macromoléculas Jiri Jonas, Universidade Federal do Rio de Janeiro, Brazil; †Department of Chemistry, Physical Chemistry I, University of Dortmund, Dortmund, Germany; ‡Ludwig Institute for Cancer Research, São Paulo, SP, Brazil; and §Departamento de Medicamentos, Faculdade de Farmácia, Universidade Federal do Rio de Janeiro, Rio de Janeiro, Brazil

ABSTRACT The main hypothesis for prion diseases is that the cellular protein (PrP^C) can be altered into a misfolded, β-sheet-rich isoform (PrP^{Sc}), which undergoes aggregation and triggers the onset of transmissible spongiform encephalopathies. Here, we investigate the effects of amino-terminal deletion mutations, $rPrP^{\Delta 51-90}$ and $rPrP^{\Delta 32-121}$, on the stability and the packing properties of recombinant murine PrP. The region lacking in $rPrP^{\Delta 51-90}$ is involved physiologically in copper binding and the other construct lacks more amino-terminal residues (from 32 to 121). The pressure stability is dramatically reduced with decreasing N-domain length and the process is not reversible for $rPrP^{\Delta 51-90}$ and $rPrP^{\Delta 32-121}$, whereas it is completely reversible for the wild-type form. Decompression to atmospheric pressure triggers immediate aggregation for the mutants in contrast to a slow aggregation process for the wild-type, as observed by Fourier-transform infrared spectroscopy. The temperature-induced transition leads to aggregation of all rPrPs, but the unfolding temperature is lower for the rPrP amino-terminal deletion mutants. The higher susceptibility to pressure of the amino-terminal deletion mutants can be explained by a change in hydration and cavity distribution. Taken together, our results show that the amino-terminal region has a pivotal role on the development of prion misfolding and aggregation.

INTRODUCTION

The prion agent, responsible for the occurrence of transmissible spongiform encephalopathies, is believed to comprise, at least in part, the prion protein (PrP) (1,2). These diseases are characterized by intense neurodegeneration caused by the presence of abnormal PrP isoforms (3). The onset of prion diseases is linked to conversion of the normal cellular conformation (named PrP^C) into an abnormal isoform, named PrP^{Sc} (from Scrapie), which is mostly insoluble, partially protease-resistant, and contains a higher β-sheet amount (4,5). Although the three-dimensional nuclear magnetic resonance (NMR) structures of several cellular mammalian PrPs have been solved (6–9), there are no available high-resolution structures of PrP^{Sc}.

All mammal PrPs share similar structural characteristics, which include a disordered amino (N)-terminal region (comprising residues 23–124) and a globular carboxyl (C)-terminal domain (residues 125–228) (10). Several point mutations associated to genetic forms of prion diseases are segregated in the C-terminal globular domain (1), so it is believed that this region is directly associated to formation of fibrils and aggregates and to propagation of disease. However, the importance of the N-terminal region should not be neglected. A recent model for the 89–175 plastic region of the prion protein assumes that this region can adopt a β-helical fold (11). Also, the 90–145 domain, which is associated with the PrP^C conversion into β-sheets (12), and the octapeptide repeats (PrP copper-binding region) are also located at the amino-terminus (13,14). The cellular location of the prion protein also corroborates the vision that the N-terminus could interact directly with exogenous PrP^{Sc} or with extracellular matrix components, such as glycosaminoglycans (15), laminin (16), or with PrP ligands (17). The importance of the N-terminal region was recently substantiated by the finding that copper (II) inhibits in vitro conversion of prion protein into amyloid fibrils (18).

The expression of amino-terminally truncated PrP in mice leads to ataxia and cerebellar lesions (19). Cellular trafficking studies of some of these deletion mutants reveal that the PrP^C isoforms are preferentially present at the plasma membrane (20). Moreover, prion protein lacking the copper-binding region (13) has been shown to be able to restore susceptibility to scrapie in PrP knockout mice (21).

High pressure has been used to investigate the $rPrP^{23-231}$ stability in comparison with rPrP aggregates (22), and we have also used this physical tool to explore the mutants' behavior in this work. The higher susceptibility to pressure of the β-sheet aggregates of rPrP could be explained by its less hydrated structure, which was corroborated by pressure perturbation calorimetry (22). The role of hydration in the folding stability of PrP and to amyloidogenicity has been reinforced by an elegant molecular dynamics study (23). High pressure favors the formation of structures with smaller volume, and application of pressure generally hydrates the hydrophobic interior of proteins (24–27). Here, we have

Submitted May 29, 2005, and accepted for publication July 13, 2005.

Address reprint requests to Jerson L. Silva, Instituto de Bioquímica Médica, Universidade Federal do Rio de Janeiro, Av. Bauhínia 400, Bloco E S10, Rio de Janeiro, 21941-590, RJ, Brazil. Tel.: 55-21-2562-6756; Fax: 55-21-3881-4155; E-mail: Jerson@bioqmed.ufrj.br.

0006-3495/05/10/2667/10 $2.00

doi: 10.1529/biophysj.105.067603

investigated the full-length recombinant murine prion protein ($rPrP^{23–231}$) stability against chemical and physical perturbations and have compared these results with the denaturation of deletion mutants of mouse rPrP, the $rPrP^{\Delta32–121}$ and the $rPrP^{\Delta51–90}$, which lack sequences with different lengths from the amino-terminal region (Scheme 1). We have investigated the secondary structure changes of the mutants induced by high pressure by Fourier-transform infrared spectroscopy (FT-IR) (28). We compare these data with previous high-pressure FT-IR results for full-length rPrP (22), and could observe differences between both mutants and the $rPrP^{23–231}$. Interestingly, although the amino-terminal deletions do not seem to contribute to the overall rPrP structural stability against all chemical perturbations applied by us, the physical treatments could differentiate the mutant's behavior from the full-length rPrP very well. Full-length rPrP displays a marked stability in comparison with the deletion mutants. After pressure-induced unfolding, the mutants acquire a higher amount of β-sheets, indicating that aggregation occurs after pressure release and, interestingly, this profile seems to be directly related to the length of the amino-terminal deletion.

MATERIALS AND METHODS

Construction, expression, and purification of recombinant prion proteins

Recombinant PCR technique (29) was used to substitute the amino acid phenylalanine to tryptophan at position 174 (F174W). We amplified cDNA fragments employing pEGFP-$PrP^{c}\Delta51–90$ and pEGFP-$PrP^{c}\Delta32–121$ (20) with internal primers (forward: 5′ CAG AAC AAC TGG GTG CAC GAC TGC 3′ and reverse: 5′ GTC GTG CAC CCA GTT GTT CTG GTT 3′) and external primers (forward: 5′ GAG GGA TCC AAA AAG CGG CCA AAG 3′ and reverse: 5′ AGA GAA TTC TCA GCT GGA TCT TCT CCC GTC 3′). The PCR fragments were cloned between *Eco*RI and *Bam*HI restriction sites in the pRSETA vector (Invitrogen). Sequencing analysis was done to check for the nucleotide substitution. The expression and purification of this protein followed the same protocol as previously described (30). For simplification, these constructs will further only be named $rPrP^{\Delta51–90}$ and $rPrP^{\Delta32–121}$ (see Scheme 1).

Reagents and protein sample

All reagents used were of analytical grade. D_2O for FT-IR was purchased from Aldrich (Seelze, Germany). For chemical- and pressure-induced denaturation, the pressure insensitive Tris buffer at 10 mM, pH 7.5, 100 mM NaCl was used. Recombinant PrPs at 5.0 μM or 10.0 μM in 10 mM sodium phosphate buffer supplemented with 100 mM NaCl, at pH 6.5, were used for circular dichroism and fluorescence spectroscopy temperature-induced transition experiments, respectively. The FT-IR measurements were performed in Tris buffer, pD 7.5, for pressure-dependent, and in phosphate buffer, pD 6.5, for temperature-dependent measurements (both buffers with 100 mM NaCl). All samples for FT-IR were lyophilized three times to remove all H_20 and then diluted to 4% (wt/wt) in 99.9% D_20 in the specified buffers.

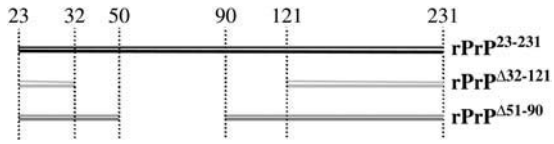

SCHEME 1 Recombinant mouse prion protein constructs. The numbers on top indicate the amino acid residue and the vertical dotted lines deliminate the regions that are lacking in the rPrP deletion mutants in comparison with full-length rPrP (*upper black line*).

Spectroscopic measurements

Light scattering and fluorescence spectra were recorded on an ISSPC1 fluorometer (ISS, Champaign, IL) or on a Varian Cary Eclipse fluorometer. Light scattering at 90° was measured illuminating the samples at 320 nm and collecting LS from 300 to 340 nm for the temperature-induced aggregation assays and a 10°C/h scanning rate was applied. The tryptophan fluorescence of $rPrP^{23–231}$, $rPrP^{\Delta51–90}$ and $rPrP^{\Delta32–121}$ was measured by exciting at 280 nm and the emission detected from 300 to 420 nm.

FT-IR spectroscopy

The FT-IR spectra were recorded with a MAGNA 550 spectrometer from Nicolet (Offenbach, Germany) equipped with a MCT (HgCdTe) detector operated at −196°C. Each spectrum was obtained by coadding 256 scans at a spectral resolution of 2 cm^{-1} and was apodized with a Happ-Genzel function. As background, the buffer spectrum was used. The spectrometer chamber was purged with dry and carbon dioxide free air. For temperature-dependent experiments, the sample chamber with 4-mm thick CaF_2 windows and an optical path length of 50 μm was used. A diamond anvil cell (High Pressure Diamond Optics, Tucson, AZ) with type IIa diamonds was used for the measurements under pressure, which were carried out between 1 bar and ~10 kbar. Powdered α-quartz was placed in the pinhole of the steel gasket, and changes in pressure were quantified by the shift of the quartz phonon band at 798 cm^{-1}. An external thermostat was used for the pressure- and temperature-dependent measurements to control the temperature to within 0.1°C. The equilibration time before each spectrum was recorded at each temperature and pressure was 15 min. Fourier self-deconvolution of the FT-IR spectra was performed with a resolution enhancement factor of 1.8 and a bandwidth of 15 cm^{-1}. Determination of peak position and curve fitting were performed with OMNIC (Nicolet, Madison, WI) and GRAMS (Galactic, Salem, NH) software, respectively. The integral intensities of the secondary structure elements of rPrP were calculated by analysis of the amide I′ vibration mode of the infrared spectrum. A peak fitting procedure using mixed Gaussian and Lorentzian peak function allows overlapping bands to be modeled as the sum of fully resolved ideal peak functions and includes peak picking, baseline fitting, and statistical results (22,28,31,32). Peak fitting was performed using an iterative method that starts with a set of initial values for the peak parameters and modifies them until the χ^2 value (reduced χ-squared, a weighted difference measure between the actual and measured data) reaches a minimum. A measure of the goodness of fits is the correlation R^2 factor (the ratio of variances between the fitted data and the average over that of the raw data over the average).

The amide I′ mode of rPrP was fitted in the range from 1695 to 1596 cm^{-1} and analyzed using six mixed Gauss-Lorentz functions. From the parameters found, the peak areas (integral intensities) of all components were calculated. The output relative peak areas of the amide I′ band (= integral intensity) have an approximate error of ±2%. Typical R^2-values of the peak fitting statistics were in the range of 98.7–99.6%.

The transitions detected were not reversible, than an analysis of the data in terms of valid thermodynamic is not appropriate.

Far-UV circular dichroism

Circular dichroism spectra of recombinant prion protein were recorded using a Jasco J-715 spectropolarimeter (Jasco, Tokyo, Japan) at 25°C, with 2.00-mm path-length cells. All spectra were subtracted from the respective buffer spectrum and collected with four accumulations each.

RESULTS

We have investigated the secondary structure content of the rPrP deletion mutants $rPrP^{\Delta 51-90}$ and $rPrP^{\Delta 32-121}$ by circular dichroism (CD) spectroscopy (Fig. 1 *A*). Both exhibit a α-helix-rich structure at physiological pH and the CD spectra are very similar to that of full-length PrP (Fig. 1 *A*). We subtracted the CD spectra of the deletion mutants from the spectrum of the recombinant rPrP to access their structural differences (Fig. 1 *A*, *inset*). The resulting spectra are almost devoid of α-helices and display a higher random coil content, as expected, because the regions lacking in the mutants are supposed to be unordered (7,9). Assuming that the deleted residues just reduce the random coil content and do not change the structure of the C-terminal core, we calculated the secondary structure content of the mutants, based on the NMR data (Protein Data Bank (PDB): 1AG2). These ''theoretical'' values are listed in Table 1.

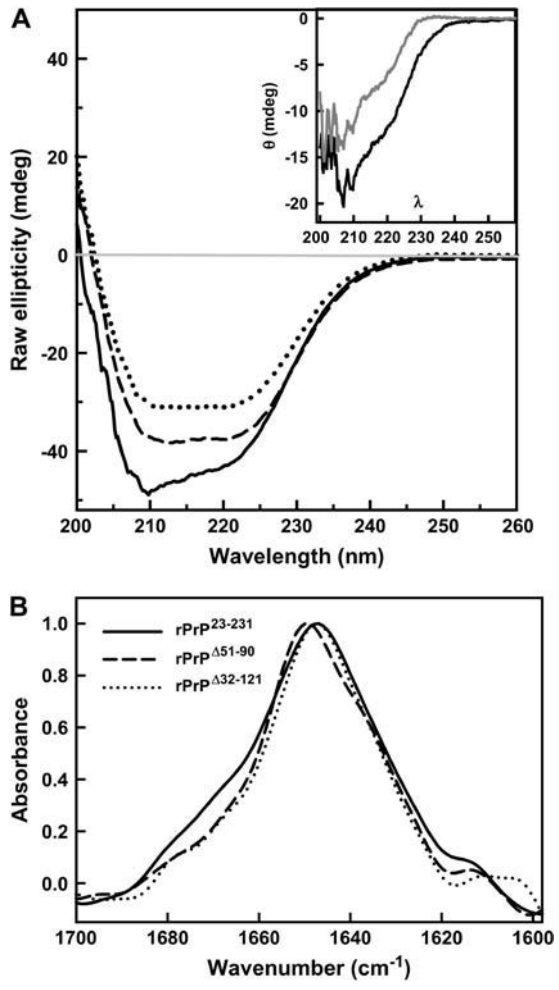

FIGURE 1 Secondary structure of $rPrP^{\Delta 51-90}$ and $rPrP^{\Delta 32-121}$ analyzed by CD and FT-IR spectroscopy. (*A*) CD spectra of $rPrP^{23-231}$ (*solid line*), $rPrP^{\Delta 51-90}$ (*dashed line*), and $rPrP^{\Delta 32-121}$ (*dotted line*) at 5.0 μM, pH 6.5. (*Inset*) Spectrum of $rPrP^{23-231}$ subtracted from $rPrP^{\Delta 32-121}$ (*solid line*) and from $rPrP^{\Delta 51-90}$ (*shaded line*) spectra. All CD and FT-IR measurements were performed at 25°C in 10 mM phosphate buffer. (*B*) Fourier self-deconvoluted FT-IR spectra of 4% (wt/wt) recombinant PrPs at pD 6.5.

To obtain detailed information on the secondary structure of $rPrP^{\Delta 32-121}$ and $rPrP^{\Delta 51-90}$, we monitored their infrared absorption spectrum at 25°C by FT-IR spectroscopy. Briefly, one can obtain information about the secondary structure components, by analysis of the IR amide I band. The amide I band (which downshifts by ~5 cm^{-1} when in D_2O as solvent and is then labeled amide I′ band), occurs between ~1700 and ~1600 cm^{-1} (28,31), and represents 76% of the C=O stretching vibration of the amide group, coupled to the C-N stretching (14%) and C-C-N deformation (10%) mode. The exact frequency of this vibration depends on the nature of the hydrogen bonding involving the amide group, and this is determined by the particular secondary structure adopted by the protein. Due to the unknown transition dipole moments of the various secondary structure elements, only relative and no absolute values for the population of conformational states can be given. Curve fitting procedure allowing a quantization of the secondary structure in the different states was performed as described in Materials and Methods.

Fig. 1 *B* compares the amide I′ region of the mutants and the wild-type prion protein. It can be seen that the spectra are slightly different. With increasing deletion, the band broadening decreases, due to the reduced random coil content. Six bands are found to contribute to the overall amide I′ area. Table 2 lists the peak positions and areas relative to the total area of the amide I′ region. The band positions and their relative contributions for rPrP are in good agreement with our earlier work without added salt (22). As expected, deletion of the N-terminal region in the rPrP modifies the relative contribution of secondary structure elements, increasing helical structures from 25.5% in the full-length rPrP over 36.9% in $rPrP^{\Delta 51-90}$ to 41.9% in $rPrP^{\Delta 32-121}$ (at 25°C). The random coil content decreases concomitantly from 48.4% in $rPrP^{121-231}$ over 33.4% in $rPrP^{\Delta 51-90}$ to 32.3% in $rPrP^{\Delta 32-121}$.

As all tryptophans in the prion protein are highly solvent exposed, we constructed both mutants with a F174W substitution, in an attempt to internalize a tryptophan moiety in the rPrP globular region, as previously reported (33). This mutation allowed us to analyze the chemical-induced transitions by fluorescence measurements. We observed by

TABLE 1 Secondary structure content of rPrP constructions

Calculated secondary structure content	$rPrP^{23-231}$ 209 residues	$rPrP^{\Delta 51-90}$ 169 residues	$rPrP^{\Delta 32-121}$ 119 + 17 residues*
β-sheets	1.9%	2.4%	2.9%
Helices	25.8%	31.9%	39.7%
Turns (β + γ)	10.1%	12.4%	15.5%
Random coil	62.2%	53.3%	41.9%

Calculated secondary structure content based on NMR data (PDB: 1AG2), assuming that the deleted residues just reduce the random coil content and do not change the structure of the C-terminal core.
*This construct maintains the histidine tag.

TABLE 2 Secondary structure content of rPrP$^{23–231}$, rPrP$^{\Delta 51–90}$, and rPrP$^{\Delta 32–121}$ in native (at 25°C) and heat-unfolded (aggregated, after 12 h after cooling from 80 to 25°C) states, as determined by FT-IR spectroscopy

	WT, native		Δ51–90, native		Δ32–121, native	
Structural assignment	Wavenumber/cm^{-1}	Area/%	Wavenumber/cm^{-1}	Area/%	Wavenumber/cm^{-1}	Area/%
Intermolecular β-sheet	1680	4.6	1679	5.5	1679	2.6
Turn	1669	11.3	1666	12.7	1668	11.4
α-Helix	1652	25.5	1652	36.9	1651	41.9
Random coil	1642	48.4	1639	33.4	1641	32.3
Intramolecular β-sheet	1627	4.2	1627	6.7	1630	9.5
Intermolecular β-sheet	1613	5.9	1613	4.8	1611	2.4
	WT, aggregated		Δ51–90, aggregated		Δ32–121, aggregated	
Structural assignment	Wavenumber/cm^{-1}	Area/%	Wavenumber/cm^{-1}	Area/%	Wavenumber/cm^{-1}	Area/%
Intermolecular β-sheet	1682	5.6	1681	8.6	1681	7.2
Turn	1670	13.9	1670	7.6	1670	10.1
α-Helix	1657	21.4	1659	14.0	1659	10.7
Random coil	1645	19.6	1646	19.1	1646	25.6
Intramolecular β-sheet	1632	25.7	1629	24.2	1630	22.5
Intermolecular β-sheet	1616	13.7	1612	26.4	1612	23.8

The estimated error in the wavenumbers is ±1 cm^{-1} and ±2% for the peak areas, as determined using different peak fitting routines giving the best fitting statistics.

FT-IR that the overall structure in the globular domain has not changed significantly, and the F174W substitution did not induce a different fold of the prion protein constructs. Summarizing, the structural results obtained for the mutants are in accordance with our expectations, assuming that the region lacking in both mutants is completely random, and using as reference the NMR data for mouse rPrP$^{121–231}$ (1AG2.pdb) (7,34).

Once having basic structural information about the murine rPrP amino-terminal deletion mutants, we started analyzing the effects of chemical and physical perturbations on these constructs and compare them with previous results for murine full-length rPrP$^{23–231}$ (22).

Effect of chemical denaturants on the structure and stability of rPrPs

The stability of all constructs against denaturing agents was analyzed at 25°C. The urea and guanidine hydrochloride unfolding isotherms monitored by fluorescence spectroscopy showed no significant difference between all curves (not shown), which is consistent with previous findings for mouse PrP$^{121–231}$ (33). The unfolding transitions of the rPrP mutants induced by urea and guanidine hydrochloride were also monitored by circular dichroism spectroscopy. Fig. 2 reveals the α-helical secondary structure content as a function of chemical denaturant concentration. We observe similar results as for the tertiary structural changes, where all rPrP constructs behave similarly upon guanidine-induced unfolding. The urea-induced transitions of the deletion mutants can not be distinguished from the one observed for full-length rPrP (data not shown), only the mean denaturation concentration required is different for both denaturing agents, as shown in Table 3. Whereas a $U_{1/2}$ value of ~6 M is observed for urea, a $G_{1/2}$ value of ~2.7 M is obtained for GdnHCl for all samples.

Hence, according to these data, the N-terminal domains 51–90 and 32–121 do not contribute to the prion protein structural stability, although they seem to be important for the putative PrP^{C} physiological role(s) (19,21).

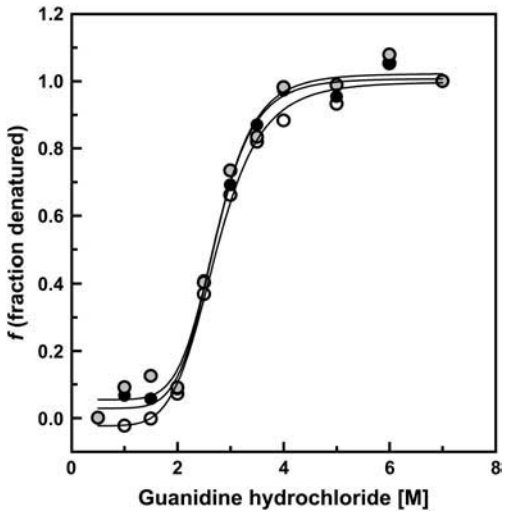

FIGURE 2 Effect of chemical denaturants on rPrP deletion mutants. The α-helical secondary structure content of the rPrPs in the presence of guanidine hydrochloride was monitored by CD spectroscopy. Raw ellipticity values at 222 nm were collected and results are displayed as fraction denatured ($f = (\varepsilon_{222nmobs} - \varepsilon_{222nminitial})/(\varepsilon_{222nmfinal} - \varepsilon_{222nminitial})$). Conditions: rPrP$^{23–231}$ (*open circles*), rPrP$^{\Delta 51–90}$ (*solid circles*), and rPrP$^{\Delta 32–121}$ (*shaded circles*) at 3.0 μM in 50 mM Tris buffer, 100 mM NaCl, pH 7.5, were incubated with denaturant for 1 h and CD spectra (2.00-mm path-length cell with 4 accumulations) were collected.

TABLE 3 Unfolding characteristics of prion protein

Prion construct	$T_{1/2}$ (°C) (CD data)	$T_{1/2}$ (°C) (LS data)	$T_{1/2}$ (°C) (FT-IR data)	$G_{1/2}$ (M) (CD data)	$U_{1/2}$ (M) (CD data)
$rPrP^{23-231}$	68.4 ± 0.6	64.2 ± 0.2	45.5 ± 0.2	2.7 ± 0.1	6.3 ± 0.3
$rPrP^{\Delta 51-90}$	64.4 ± 0.5	57.7 ± 0.1	43.0 ± 0.1	2.7 ± 0.1	6.2 ± 0.1
$rPrP^{\Delta 32-121}$	64.2 ± 0.2	56.6 ± 0.2	40.1 ± 0.8	2.7 ± 0.1	6.2 ± 0.2

The medium values for the transitions were calculated from the respective set of data for each measurement. The curves were fitted assuming a two-state transition with a sigmoidal equation.

Thermal denaturation of recombinant mouse PrPs

Further, we performed measurements of the thermal-induced transitions for the full-length and mutant rPrPs and monitored the decrease in α-helical secondary structure by CD (Fig. 3 *A*). The raw ellipticity value at 222 nm, which is present in proteins containing a high α-helical content (35), was monitored during the temperature increase from 25 to ~90°C. We observed that, although $rPrP^{\Delta 32-121}$ and $rPrP^{\Delta 51-90}$ display a similar unfolding profile within the experimental error, with a $T_{1/2}$ for unfolding at ~64°C, the $rPrP^{23-231}$ is significantly more thermally stable ($T_{1/2}$ = 68°C). The thermal transition was not completely reversible after return to 25°C. We have then monitored the rPrP mutant's aggregation by the increase in light scattering as a function of temperature (Fig. 3 *B*). In agreement with the CD results, we observed that both mutants aggregate at lower temperatures compared to full-length rPrP (Table 3).

To investigate the effect of temperature on the secondary structure of prion protein, we also measured the heat-induced changes in the amide I′ region of the infrared spectrum in the temperature range from 20 to 80°C with a scanning rate of 20°C/h (Fig. 4). Selected FT-IR spectra for the smaller construct, $rPrP^{\Delta 32-121}$, are shown in Fig. 4 *A*. We verified that protein aggregation takes place above 41°C, as can be seen from the appearance and further increase of the IR intensities at 1612 and 1681 cm^{-1}, respectively, which are characteristic of intermolecular antiparallel β-sheets (36). The relative content of secondary structure elements of $rPrP^{\Delta 51-90}$ and $rPrP^{\Delta 32-121}$ are depicted in Fig. 4, *B* and *C*, respectively (see also Table 2). The unfolding temperature ($T_{1/2}$) of $rPrP^{\Delta 51-90}$ is ~43°C, and $rPrP^{\Delta 32-121}$ unfolds at ~40°C, whereas the full-length rPrP unfolds at ~46°C (Table 3). During the unfolding and aggregation, the wild-type prion protein loses ~16% of α-helices (from 25.5 in the native state to 21.4% in the aggregated state) and ~60% of disordered structures (from 48.4 to 19.6%) forming non-native β-sheets; ~1/2 of the residues (45%) are involved in the β-sheet formation (at 25°C, 12 h after the cooling from 80°C). With decreasing N-terminal domain size, the stability of α-helices decreases dramatically: ~62% of α-helices undergo the transition to β-sheets in the case of $rPrP^{\Delta 51-90}$, whereas $rPrP^{\Delta 32-121}$ loses ~75% of its α-helices upon aggregation. The content of β-sheets is higher in the mutants,

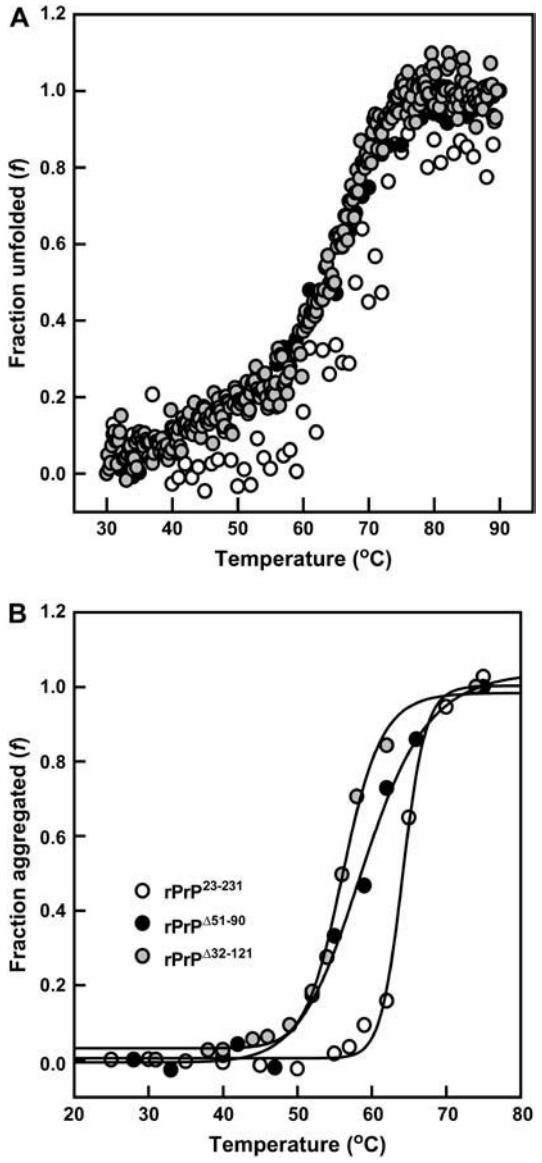

FIGURE 3 Temperature-induced unfolding of rPrP's. (*A*) CD measurements showing loss of α-helical secondary structure (calculated as in Fig. 2) as a function of temperature. The heating rate was 1°C/min. (*B*) Temperature-induced aggregation measured by the increase in light scattering at 320 nm. The heating rate was 10°C/h and LS spectra were collected 5 min after incubation at each temperature. $rPrP^{23-231}$ (*open circles*), $rPrP^{\Delta 51-90}$ (*solid circles*) and $rPrP^{\Delta 32-121}$ (*shaded circles*) at 5.0 μM (for CD) and 10.0 μM (for LS) in 10 mM phosphate buffer, pH 6.5.

when compared to $rPrP^{23-231}$: ~59% of $rPrP^{\Delta 51-90}$ and ~54% of $rPrP^{\Delta 32-121}$ residues are involved in the conversion into β-sheet-rich species of the prion protein. Obviously, the flexible N-domain of prion protein protects the globular C-domain against intermolecular β-sheet formation (and hence fibrillogenesis), possibly via loose contacts with the protein surface and thus sterical protection.

Upon cooling to room temperature, the aggregation bands remained unchanged, indicating that the temperature-induced

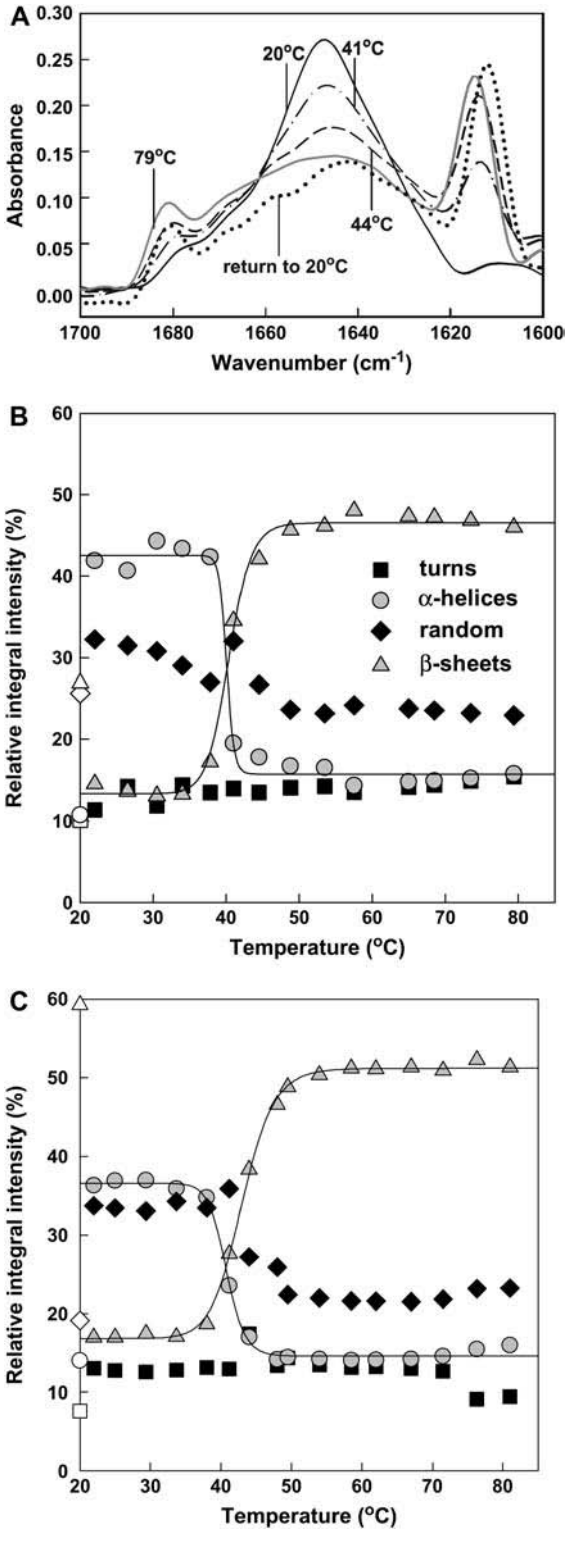

FIGURE 4 Temperature-induced aggregation of rPrPs measured by FT-IR spectroscopy. (*A*) Selected Fourier self-deconvoluted FT-IR spectra of the $rPrP^{\Delta 32-121}$ temperature-induced transition. Relative intensity of $rPrP^{\Delta 32-121}$ (*B*) and $rPrP^{\Delta 51-90}$ (*C*) secondary structure components as a function of temperature. All open symbols correspond to the respective secondary structure component 12 h after cooling to 25°C. The error in determination of the secondary structure elements from the relative peak areas of the amide I′ band (integral intensities) from different runs is ~±2%, smaller than the size of the symbols.

transition of the prion mutants is irreversible (Fig. 4, *A* and *B*, *open symbols*), as observed for mouse full-length rPrP (22).

The measured middle temperature ($T_{1/2}$) of unfolding is different for both techniques (Table 3), but we observe the same trend in terms of heat resistance and aggregation. This difference is due to the different sensitivity of the methods used. In the FT-IR measurements, a much higher concentration was used in comparison to that in the CD measurements (see Materials and Methods section). Taken together, these results suggest that the N-terminal region may contribute in part to the overall prion protein stability.

Effect of high pressure on the structure and stability of recombinant mutant PrPs

To investigate the unfolding and aggregation profile of the rPrP deletion mutants, $rPrP^{\Delta 32-121}$ and $rPrP^{\Delta 51-90}$ in greater depth, we analyze their stability against pressure and compare these results with the pressure-induced unfolding of $rPrP^{23-231}$ (22) (Fig. 5). Pressure was increased from 0.001 to ~13 kbar and the changes in the amide I′ vibration mode at 25°C were detected. Exemplary, selected FT-IR spectra of $rPrP^{\Delta 51-90}$ as a function of pressure are shown in Fig. 5 *A*. The secondary structure changes upon isothermal $rPrP^{\Delta 51-90}$ and $rPrP^{\Delta 32-121}$ pressurization are clearly visualized in Fig. 5, *B* and *C*, respectively. In the case of full-length rPrP, we observe the unfolding above 4.5 kbar with a $p_{1/2} = 5.4 \pm 0.2$ kbar, indicated by typical changes in the amide I′ band region: The band becomes broader and the intensity of the main peak decreases and shifts to lower wavenumbers, pointing to a decrease in α-helical structures (22). Upon unfolding, $rPrP^{23-231}$ loses ~54% of the α-helices, only 12% of the protein remain helical at 10 kbar. Concomitantly, turns, random coil, and β-sheet elements increase slightly. When we compare the pressure sensitivity of the mutants with that of the full-length prion protein, we find that the unfolding pressure shifts drastically to lower values. In the case of $rPrP^{\Delta 51-90}$, unfolding is completed above ~2.2 kbar with a $p_{1/2} = 1.23$ kbar, and for the smaller construct, $rPrP^{\Delta 32-121}$, the unfolding is completed above ~2.0 kbar, with a $p_{1/2} = 0.74$ kbar. $rPrP^{\Delta 32-121}$ seems to be extremely unstable under pressure; unfolding takes place already after the closing of the diamond anvil cell (which is connected with an inevitable small pressure increase in the range of few ten bars, needed to get the high-pressure cell sealed), as can be seen from the initial values depicted in Fig. 5 *C*. The unfolding pathway follows a scenario similar to that of full-length prion protein: $rPrP^{\Delta 51-90}$ loses ~55% of the α-helices with only 16.5% remaining at 9 kbar; the α-helical content of $rPrP^{\Delta 32-121}$ decreases by ~58% (from 41.9% at 1 bar to 17.4% at 9 kbar) during the pressure-induced unfolding. Concomitantly, we observe an increasing content of random

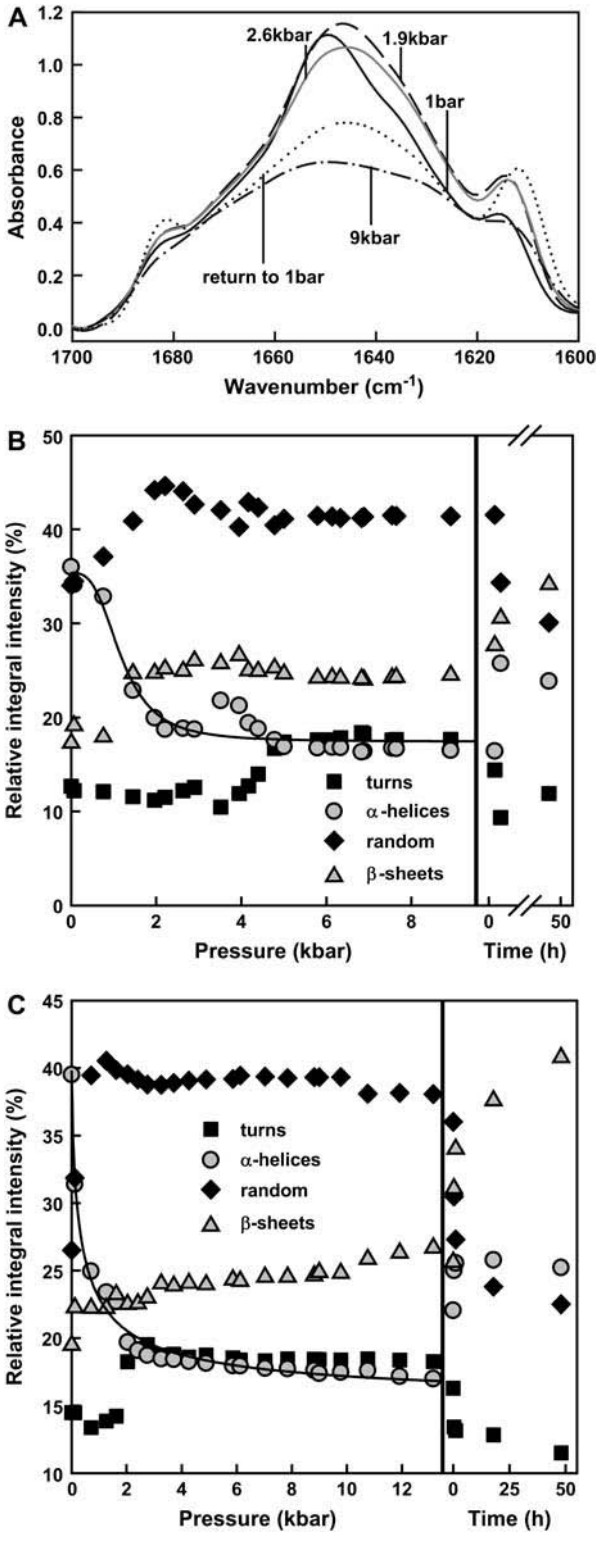

FIGURE 5 Pressure-induced transition of rPrP deletion mutants. (*A*) Selected FSD FT-IR spectra of $rPrP^{\Delta 51-90}$ (Tris buffer, pD 7.5, 100 mM NaCl) as a function of pressure at 25°C. Relative intensity of $rPrP^{\Delta 51-90}$ (*B*) and $rPrP^{\Delta 32-121}$ (*C*) secondary structure components as a function of pressure. The right panels in each plot follow the percentage of secondary structure components after return to 1 bar.

coil structures and, surprisingly, the amount of β-sheets increases, indicating that protein aggregation is enhanced under pressure. The amount of β-sheet structures, thus, increases with decreasing N-domain size: ~19% in $rPrP^{23-231}$, ~25% in $rPrP^{\Delta 51-90}$ and ~27% $rPrP^{\Delta 32-121}$ at 9 kbar. Such kind of behavior was also observed recently with the Syrian hamster $rPrP^{90-231}$ (37).

The isothermal pressure-induced unfolding transitions were not reversible (see *right-hand side* of Fig. 5, *B* and *C*), as in the case of full-length rPrP (within the same time range). Strikingly, the deletion mutants aggregated immediately after return to atmospheric pressure at 25°C (Fig. 6). The IR bands at ~1613 and 1682 cm^{-1} increase drastically after pressure release, and this increase, indicative of progressing aggregation, is directly related to the size of the amino-terminal deletion. The $rPrP^{\Delta 32-121}$, which lacks most of the rPrP disordered region (34), aggregates more rapidly and more extensively than $rPrP^{\Delta 51-90}$ upon pressure release. In Fig. 6, the infrared spectra after return to atmospheric pressure of the prion protein constructs studied here are shown for comparison. It is interesting to note that, even full-length rPrP aggregates at 25°C after return to 1 bar, but this process is much slower than for the mutants lacking parts of the N-terminus. Whereas the full-length rPrP aggregation takes ~24 h to occur after release of pressure, the aggregation of the two mutants is already massive in the first hour after decompression. The mutant with larger deletion ($rPrP^{\Delta 32-121}$) is the one that aggregates faster.

DISCUSSION

Our goal was to understand how the disordered amino-terminal region of the prion protein affects the stability and hence aggregation behavior of the protein. Our main finding was that rPrP mutants lacking parts of this region behave

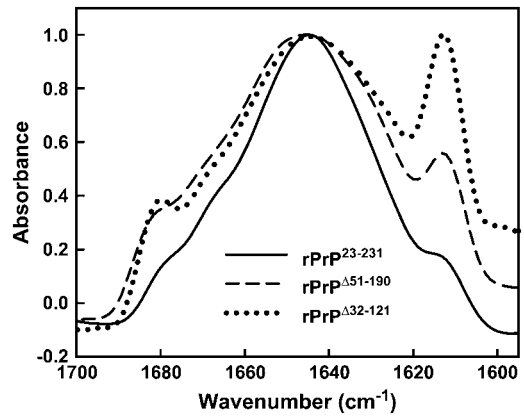

FIGURE 6 Amino-terminal domain affects pressure-induced prion aggregation. Infrared spectra (amide I′ range) of the rPrP constructs after pressure release: $rPrP^{23-231}$ (*solid line*), $rPrP^{\Delta 51-90}$ (*dashed line*), and $rPrP^{\Delta 32-121}$ (*dotted line*), 1 h after return to 1 bar. All measurements were performed at 25°C, 4% (wt/wt) protein concentration at pD 7.5 with 100 mM NaCl.

differently from full-length rPrP against physical treatments. On the contrary, denaturation of $rPrP^{23-231}$, $rPrP^{\Delta 32-121}$, and $rPrP^{\Delta 51-90}$ by chemical agents, such as urea and guanidinium hydrochloride, exhibits a similar profile for all the proteins studied.

The amino-terminal region of PrP, which comprehends residues 23 to 121 (10), is unstructured (6), and most of the point mutations associated to hereditary forms of prion diseases are segregated in the C-terminal, globular folded domain (1). However, a great part of this flexible region is involved in the structural conversion from PrP^{C} to PrP^{Sc}, as verified by molecular modeling (11,12). Moreover, the hydrophobic region (residues 106 to 126) of the PrP is toxic to cells in culture (38). It has also been recently verified that this region can alter the conformation of protease-resistant PrP (PrP-res) generated in an in vitro cell-free assay, suggesting that the PrP flexible amino-terminus is also involved in transmissible spongiform encephalopathies pathogenesis and cross-species transmissible spongiform encephalopathies transmission (39). Other macromolecules have been reported to be involved in the PrP^{C} to PrP^{Sc} conversion, such as nucleic acids (40,41) and glycosaminoglycans (15). The binding of nucleic acid to recombinant prion protein seems to involve both the N-terminus and the globular C-terminal domain (L. M. T. R. Lima, Y. Cordeiro, and J. L. Silva, 2005, unpublished results). Nucleic acid binding competes with the binding of small molecules (42).

Thermal-induced unfolding of murine rPrP deletion mutants gives rise to increased β-sheet content at temperatures above ~40°C, and to a concomitant decrease in the amount of α-helix and random coils. Whereas the $T_{1/2}$ value for full-length rPrP is higher, the aggregation profile as a function of temperature increase is similar to the mutant's behavior. Obviously, the flexible, unlinked, N-domain of the prion protein contributes to the stability of the globular C-domain against intermolecular β-sheet formation, possibly via loose contacts with the protein surface and, hence, sterical screening of the molecule. Such a scenario seems to be even more likely in a crowded cell environment.

The use of pressure permits one to isolate alternative structural conformers from the folding pathway, such as intermediates on the route of aggregation (27,43–46). For example, it was recently verified that recombinant $ShaPrP^{90-231}$ undergoes aggregation upon pressurization (37) and that pressure promoted formation of amyloid aggregates of insulin at conditions that normally do not favor aggregation (47). These observations are very interesting and striking, because normally pressure leads to dissociation of aggregates (48) or oligomeric proteins (49), or to unfolding of protein monomers (24,45).

The pressure-induced unfolding transition of $rPrP^{\Delta 32-121}$ and $rPrP^{\Delta 51-90}$ is very distinct from the $rPrP^{23-231}$ transition (22), which is, probably, due to differences in packing and hydration of these prion protein constructs. When we compare the pressure sensitivity of the mutants with that of the full-length prion protein, we find that the unfolding pressure shifts drastically to lower values. The midpoint of the transition of $rPrP^{23-231}$ is found to be ~5.4 kbar, which is much higher than the values found for the two mutants. In the case of $rPrP^{\Delta 51-90}$, the unfolding is completed above ~2.2 kbar with a $p_{1/2} = 1.23$ kbar, and for the smaller construct $rPrP^{\Delta 32-121}$, the unfolding is completed above ~2.0 kbar, with $p_{1/2} = 0.74$ kbar at 25°C. The amount of β-sheets in the denatured, unfolded state increases with decreasing N-domain size. We note that the pressure-induced unfolding transitions are not reversible: Upon pressure release, both mutants form intermolecular β-sheets, with $rPrP^{\Delta 32-121}$, which lacks most of the rPrP disordered region, aggregating more rapidly and extensively than $rPrP^{\Delta 51-90}$ (immediately after ambient pressure is restored). Pressure-induced aggregation was also observed for the recombinant human interferon-γ, after release of pressure at 25°C (50).

Even wild-type rPrP aggregates after return to ambient pressure, but much slower. Here, we observe a reversibility of the pressure-induced unfolding after release of pressure, and only after ~36 h the aggregation bands become visible in the FT-IR spectra. Previously, we could analyze the reversible transitions induced by pressure in terms of volume and free-energy diagrams (22). Because of the irreversible character of the pressure denaturation of the mutants, this could not be pursued for them. The reversibility is obtained for the wild-type form because the N $\leftrightarrow$ U transitions for α-rPrP and β-rPrP are not connected at equilibrium and two unfolded species (U and U') were part of the diagram (22). In contrast, a decrease in the energy barrier between the different unfolded species would explain the fast aggregation of the mutants. Therefore, the equilibrium is quite reversible in the time frame of the experiment for the wild-type and highly irreversible for the mutants. This is more remarkable for the lengthier deletion ($rPrP^{\Delta 32-121}$). Therefore, the N-domain would have a crucial role in the modulation of the magnitude of this kinetic barrier. It is very likely that other molecules act on this barrier including nucleic acids, chaperones, and other macromolecules (15,40–42,51).

The removal of the N-terminus hence influences the secondary and, possibly, tertiary structure in such a way, that it reduces its stability against pressure also. Probably, the absence of the N-terminal region weakens the protein structure, allowing increased penetration of water into the core of molecule and formation of disordered structures, which, when exposed, are prone to aggregate more easily. Tight and dynamical hydration sites were shown to have a key role in structural stability of the prion protein (23). Thus, the higher susceptibility to pressure of the amino-terminal deletion mutants can be explained by a change in hydration and cavity distribution.

We thank Emerson R. Gonçalves for excellent technical support. We thank Prof. Pedro L. Oliveira for allowing us to use the Varian Cary Eclipse spectrofluorometer.

This work was supported by grants from Conselho Nacional de Desenvolvimento Científico e Tecnológico (CNPq), FINEP, Fundação de

Amparo à Pesquisa do Estado do Rio de Janeiro (FAPERJ), and Coordenação de Aperfeiçoamento de Pessoal de Nível Superior (CAPES) of Brazil to J.L.S. and D.F., by an international grant from the International Centre for Genetic Engineering and Biotechnology (ICGEB) to J.L.S., by a grant from Fundação Universitária José Bonifácio (FUJB) to L.M.T.R.L., and by a grant from the Deutsche Forchungsgemeinschaft (DFG-FOR 436) to R.W.

REFERENCES

1. Prusiner, S. B. 1998. Prions. *Proc. Natl. Acad. Sci. USA.* 95:13363–13383.
2. Aguzzi, A., and M. Polymenidou. 2004. Mammalian prion biology: one century of evolving concepts. *Cell.* 116:313–327.
3. Caughey, B. 2001. Interactions between prion protein isoforms: the kiss of death? *Trends Biochem. Sci.* 26:235–242.
4. Caughey, B. W., A. Dong, K. S. Bhat, D. Ernst, S. F. Hayes, and W. S. Caughey. 1991. Secondary structure analysis of the scrapie-associated protein PrP 27–30 in water by infrared spectroscopy. *Biochemistry.* 30:7672–7680.
5. Pan, K.-M., M. Baldwin, J. Nguyen, M. Gasset, A. Serban, D. Groth, I. Mehlhorn, Z. Huang, R. J. Fletterick, F. E. Cohen, and S. B. Prusiner. 1993. Conversion of alpha-helices into beta-sheets features in the formation of the scrapie prion proteins. *Proc. Natl. Acad. Sci. USA.* 90: 10962–10966.
6. Donne, D. G., J. H. Viles, D. Groth, I. Mehlhorn, T. L. James, F. E. Cohen, S. B. Prusiner, P. E. Wright, and J. H. Dyson. 1997. Structure of the recombinant full-length hamster prion protein PrP (29–231): the N-terminus is highly flexible. *Proc. Natl. Acad. Sci. USA.* 94:13452–13457.
7. Riek, R., S. Hornemann, G. Wider, R. Glockshuber, and K. Wüthrich. 1997. NMR characterization of the full-length recombinant murine prion protein, mPrP(23–231). *FEBS Lett.* 413:282–288.
8. Lopez-Garcia, F., R. Zahn, R. Riek, and K. Wüthrich. 2000. NMR structure of the bovine prion protein. *Proc. Natl. Acad. Sci. USA.* 97: 8334–8339.
9. Zahn, R., A. Liu, T. Luhrs, R. Riek, C. von Schrötter, F. Lopez-Garcia, M. Billeter, L. Calzolai, G. Wider, and K. Wüthrich. 2000. NMR solution structure of the human prion protein. *Proc. Natl. Acad. Sci. USA.* 97:145–150.
10. Wüthrich, K., and R. Riek. 2001. Three-dimensional structures of prion proteins. *Adv. Protein Chem.* 57:55–82.
11. Govaerts, C., H. Wille, S. B. Prusiner, and F. E. Cohen. 2004. Evidence for assembly of prions with left-handed beta-helices into trimers. *Proc. Natl. Acad. Sci. USA.* 101:8342–8347.
12. Huang, Z., S. B. Prusiner, and F. E. Cohen. 1996. Scrapie prions: a three-dimensional model of an infectious fragment. *Fold. Des.* 1: 13–19.
13. Viles, J. H., F. E. Cohen, S. B. Prusiner, D. B. Goodin, P. E. Wright, and H. J. Dyson. 1999. Copper binding to the prion protein: structural implications of four identical cooperative binding sites. *Proc. Natl. Acad. Sci. USA.* 96:2042–2047.
14. Brown, D. R., K. Qin, J. W. Herms, A. Madlung, J. Manson, R. Strome, P. E. Fraser, T. Kruck, A. von Bohlen, W. Schulz-Schaeffer, A. Giese, D. Westaway, and H. Kretzschmar. 1997. The cellular prion protein binds copper in vivo. *Nature.* 390:684–687.
15. Priola, S. A., and B. Caughey. 1994. Inhibition of scrapie-associated PrP accumulation. Probing the role of glycosaminoglycans in amyloidogenesis. *Mol. Neurobiol.* 8:113–120.
16. Graner, E., A. F. Mercadante, S. M. Zanata, O. V. Forlenza, A. L. Cabral, S. S. Veiga, M. A. Juliano, R. Roesler, R. Walz, A. Minetti, I. Izquierdo, V. R. Martins, and R. R. Brentani. 2000. Cellular prion protein binds laminin and mediates neuritogenesis. *Brain Res. Mol. Brain Res.* 76:85–92.
17. Martins, V. R., R. Linden, M. A. Prado, R. Walz, A. C. Sakamoto, I. Izquierdo, and R. R. Brentani. 2002. Cellular prion protein: on the road for functions. *FEBS Lett.* 512:25–28.
18. Bocharova, O. V., L. Breydo, V. V. Salnikov, and I. V. Baskakov. 2005. Copper(II) inhibits in vitro conversion of prion protein into amyloid fibrils. *Biochemistry.* 44:6776–6787.
19. Shmerling, D., I. Hegyi, M. Fischer, T. Blattler, S. Brandner, J. Gotz, T. Rulicke, E. Flechsig, A. Cozzio, C. von Mering, C. Hangartner, A. Aguzzi, and C. Weissmann. 1998. Expression of amino-terminally truncated PrP in the mouse leading to ataxia and specific cerebellar lesions. *Cell.* 93:203–214.
20. Lee, K. S., A. C. Magalhães, S. M. Zanata, R. R. Brentani, V. R. Martins, and M. A. Prado. 2001. Internalization of mammalian fluorescent cellular prion protein and N-terminal deletion mutants in living cells. *J. Neurochem.* 79:79–87.
21. Flechsig, E., D. Shmerling, I. Hegyi, A. J. Raeber, M. Fischer, A. Cozzio, C. von Mering, A. Aguzzi, and C. Weissmann. 2000. Prion protein devoid of the octapeptide repeat region restores susceptibility to scrapie in PrP knockout mice. *Neuron.* 27:399–408.
22. Cordeiro, Y., J. Kraineva, R. Ravindra, L. M. Lima, M. P. Gomes, D. Foguel, R. Winter, and J. L. Silva. 2004. Hydration and packing effects on prion folding and beta-sheet conversion. High pressure spectroscopy and pressure perturbation calorimetry studies. *J. Biol. Chem.* 279: 32354–32359.
23. De Simone, A., G. D. Dodson, C. S. Verma, A. Zagari, and F. Fraternali. 2005. Prion and water: tight and dynamical hydration sites have a key role in structural stability. *Proc. Natl. Acad. Sci. USA.* 102:7535–7540.
24. Oliveira, A. C., L. P. Gaspar, A. T. da Poian, and J. L. Silva. 1994. Arc repressor will not denature under pressure in the absence of water. *J. Mol. Biol.* 240:184–187.
25. Royer, C. A. 2002. Revisiting volume changes in pressure-induced protein unfolding. *Biochim. Biophys. Acta.* 25:201–209.
26. Silva, J. L., D. Foguel, and C. Royer. 2001. Pressure provides new insights into protein folding, dynamics, and structure. *Trends Biochem. Sci.* 26:612–618.
27. Foguel, D., and J. L. Silva. 2004. New insights into the mechanisms of protein misfolding and aggregation in amyloidogenic diseases derived from pressure studies. *Biochemistry.* 43:11361–11370.
28. Byler, D. M., and H. Susi. 1986. Examination of the secondary structure of proteins by deconvolved FTIR spectra. *Biopolymers.* 25: 469–487.
29. Ausubel, F. M., R. Brent, R. E. Kingston, D. D. Moore, J. D. Seidman, J. A. Smith, and K. Struhl. 1993. Current Protocols in Molecular Biology, Wiley Interscience, New York.
30. Zahn, R., C. von Schrötter, and K. Wüthrich. 1997. Human prion proteins expressed in *Escherichia coli* and purified by high-affinity column refolding. *FEBS Lett.* 417:400–404.
31. Panick, G., R. Malessa, and R. Winter. 1999. Differences between the pressure- and temperature-induced denaturation and aggregation of beta-lactoglobulin A, B, and AB monitored by FT-IR spectroscopy and small-angle x-ray scattering. *Biochemistry.* 38:6512–6519.
32. Herberhold, H., S. Marchal, R. Lange, C. H. Scheyhing, R. F. Vogel, and R. Winter. 2003. Characterization of the pressure-induced intermediate and unfolded state of red-shifted green fluorescent protein—a static and kinetic FTIR, UV/VIS and fluorescence spectroscopy study. *J. Mol. Biol.* 330:1153–1164.
33. Wildegger, G., S. Liemann, and R. Glockshuber. 1999. Extremely rapid folding of the C-terminal domain of the prion protein without kinetic intermediates. *Nat. Struct. Biol.* 6:550–553.
34. Riek, R., S. Hornemann, G. Wider, M. Billeter, R. Glockshuber, and K. Wüthrich. 1996. NMR structure of the mouse prion protein domain PrP(121–321). *Nature.* 382:180–182.
35. Johnson, W. C., Jr. 1988. Secondary structure of proteins through circular dichroism spectroscopy. *Annu. Rev. Biophys. Biophys. Chem.* 17:145–166.
36. Ismail, A. A., H. H. Mantsch, and P. T. T. Wong. 1992. Aggregation of chymotrypsinogen: portrait by infrared spectroscopy. *Biochim. Biophys. Acta.* 1121:183–188.

37. Torrent, J., M. T. Alvarez-Martinez, M. C. Harricane, F. Heitz, J. P. Liautard, C. Balny, and R. Lange. 2004. High pressure induces scrapie-like prion protein misfolding and amyloid fibril formation. *Biochemistry*. 43:7162–7170.

38. Brown, D. R., B. Schmidt, and H. A. Kretzschmar. 1996. Role of microglia and host prion protein in neurotoxicity of a prion protein fragment. *Nature*. 380:345–347.

39. Lawson, V. A., S. A. Priola, K. Meade-White, M. Lawson, and B. Chesebro. 2004. Flexible N-terminal region of prion protein influences conformation of protease-resistant prion protein isoforms associated with cross-species scrapie infection in vivo and in vitro. *J. Biol. Chem.* 279:13689–13695.

40. Cordeiro, Y., F. Machado, L. Juliano, M. A. Juliano, R. R. Brentani, D. Foguel, and J. L. Silva. 2001. DNA converts cellular prion protein into the beta-sheet conformation and inhibits prion peptide aggregation. *J. Biol. Chem.* 276:49400–49409.

41. Deleault, N. R., R. W. Lucassen, and S. Supattapone. 2003. RNA molecules stimulate prion protein conversion. *Nature*. 425:717–720.

42. Cordeiro, Y., L. M. Lima, M. P. Gomes, D. Foguel, and J. L. Silva. 2004. Modulation of prion protein oligomerization, aggregation, and beta-sheet conversion by 4,4′-dianilino-1,1′-binaphthyl-5,5′-sulfonate (bis-ANS). *J. Biol. Chem.* 279:5346–5352.

43. Silva, J. L., and G. Weber. 1993. Pressure stability of proteins. *Annu. Rev. Phys. Chem.* 44:89–113.

44. Mozhaev, V. V., K. Heremans, J. Frank, P. Masson, and C. Balny. 1996. High pressure effects on protein structure and function. *Proteins*. 24:81–91.

45. Winter, R., and W. Dzwolak. 2004. Temperature-pressure configurational landscape of lipid bilayers and proteins. *Cell. Mol. Biol.* 50: 397–417.

46. Ferrão-Gonzales, A. D., S. O. Souto, J. L. Silva, and D. Foguel. 2000. The preaggregated state of an amyloidogenic protein: hydrostatic pressure converts native transthyretin into the amyloidogenic state. *Proc. Natl. Acad. Sci. USA*. 97:6445–6450.

47. Jansen, R., S. Grudzielanek, W. Dzwolak, and R. Winter. 2004. High pressure promotes circularly shaped insulin amyloid. *J. Mol. Biol.* 338:203–206.

48. Foguel, D., M. C. Suarez, A. D. Ferrão-Gonzales, T. C. Porto, L. Palmieri, C. M. Einsiedler, L. R. Andrade, H. A. Lashuel, P. T. Lansbury, J. W. Kelly, and J. L. Silva. 2003. Dissociation of amyloid fibrils of alpha-synuclein and transthyretin by pressure reveals their reversible nature and the formation of water-excluded cavities. *Proc. Natl. Acad. Sci.USA*. 100:9831–9836.

49. Balny, C., P. Masson, and K. Heremans. 2002. High pressure effects on biological macromolecules: from structural changes to alteration of cellular processes. *Biochim. Biophys. Acta*. 1595:3–10.

50. Goossens, K., J. Haelewyn, F. Meersman, M. De Ley, and K. Heremans. Pressure- and temperature-induced unfolding and aggregation of recombinant human interferon-gamma: a Fourier transform infrared spectroscopy study. *Biochem. J.* 370:529–35.

51. Nandi, P. K., and J. C. Nicole. 2004. Nucleic acid and prion protein interaction produces spherical amyloids which can function in vivo as coats of spongiform encephalopathy agent. *J. Mol. Biol.* 344: 827–837.